Emergent Chiral Spin State in the Mott Phase of a Bosonic Kane-Mele-Hubbard Model

Kirill Plekhanov,[1,2] Ivana Vasić,[3] Alexandru Petrescu,[4] Rajbir Nirwan,[5] Guillaume Roux,[1] Walter Hofstetter,[5] and Karyn Le Hur[2]

[1]*LPTMS, CNRS, Univ. Paris-Sud, Université Paris-Saclay, 91405 Orsay, France*
[2]*Centre de Physique Théorique, Ecole Polytechnique, CNRS, Université Paris-Saclay, F-91128 Palaiseau, France*
[3]*Scientific Computing Laboratory, Center for the Study of Complex Systems, Institute of Physics Belgrade, University of Belgrade, 11080 Belgrade, Serbia*
[4]*Department of Electrical Engineering, Princeton University, Princeton, New Jersey 08544, USA*
[5]*Institut für Theoretische Physik, Goethe-Universität, 60438 Frankfurt/Main, Germany*

(Received 28 July 2017; revised manuscript received 13 November 2017; published 10 April 2018)

Recently, the frustrated XY model for spins $1/2$ on the honeycomb lattice has attracted a lot of attention in relation with the possibility to realize a chiral spin liquid state. This model is relevant to the physics of some quantum magnets. Using the flexibility of ultracold atom setups, we propose an alternative way to realize this model through the Mott regime of the bosonic Kane-Mele-Hubbard model. The phase diagram of this model is derived using bosonic dynamical mean-field theory. Focusing on the Mott phase, we investigate its magnetic properties as a function of frustration. We do find an emergent chiral spin state in the intermediate frustration regime. Using exact diagonalization we study more closely the physics of the effective frustrated XY model and the properties of the chiral spin state. This gapped phase displays a chiral order, breaking time-reversal and parity symmetry, but is not topologically ordered (the Chern number is zero).

DOI: 10.1103/PhysRevLett.120.157201

The last few decades have seen growing interest in the quest for exotic spin states [1]. Significant progress has been made both from the theoretical and experimental sides [2–4]. The best candidates are found in two-dimensional systems. Disordered phases are expected to occur in complex geometries, such as the kagome lattice [5–8], or in frustrated bipartite lattices, such as the square lattice with second-neighbor couplings [9,10]. Among basic lattices, the honeycomb hosts free Majorana fermions due to Kitaev anisotropic interactions [11], and raises questions when starting from the Hubbard model [12–14]. In such context and motivated by quantum magnets [15], frustrated Heisenberg models on the honeycomb lattice have been recently explored [16–29]. In parallel, some materials were found to realize the XXZ version of this model [30], and theoretical and numerical studies suggested that the XY version possibly hosted a chiral spin liquid state, with seemingly contradictory results [31–38]. As suggested in Ref. [39], in the intermediate frustration regime the ground-state physics could be mapped to a fermionic Haldane model [40] with topological Bloch bands at a mean-field level, as a result of Chern-Simons (ChS) gauge fields [41–45]. However, the topological nature of this spin state is still elusive.

Our objectives are twofold in this Letter. Motivated by cold atom experiments [46,47], we first study the phase diagram of the bosonic Kane-Mele-Hubbard (BKMH) model using bosonic dynamical mean-field theory (B-DMFT) [48–54]. The Kane-Mele model [55] is the standard model with spin-orbit coupling that displays a $\mathbb{Z}_2$ topological classification. Still, it has not yet been studied for interacting bosons, and for interacting fermions at the Mott transition it becomes magnetically ordered in the xy plane, with quantum fluctuations stabilizing the Neel ordering [56–58]. We explore the Mott regime of this model and show that it allows for a tunable realization of the frustrated XY model on the honeycomb lattice. Second, we use exact diagonalization (ED) and theoretical arguments to study the resulting XY model. We observe that an intermediate frustration regime hosts a chiral spin state with spontaneously broken time-reversal ($\mathcal{T}$) and parity ($\mathcal{P}$) symmetries, associated with antiferromagnetic ordering and the onset of local currents. Based on the calculation of the Chern number, we conclude that this state has no intrinsic topological order.

We start our analysis with the bosonic version of the Kane-Mele model [55] on the honeycomb lattice [Fig. 1(a)], which contains two species of bosons labeled by $\sigma = \uparrow, \downarrow$. In the presence of repulsive Bose-Hubbard interactions, the Hamiltonian reads

$$H = -t_1 \sum_{\sigma,\langle ij\rangle} [b^\dagger_{\sigma,\mathbf{r}_i} b_{\sigma,\mathbf{r}_j} + \text{H.c.}] + i t_2 \sum_{\sigma,\langle\langle ik\rangle\rangle} \nu^\sigma_{ik} [b^\dagger_{\sigma,\mathbf{r}_i} b_{\sigma,\mathbf{r}_k} - \text{H.c.}] + \frac{U}{2} \sum_{\sigma,i} n_{\sigma,\mathbf{r}_i}(n_{\sigma,\mathbf{r}_i} - 1) + U_{\uparrow\downarrow} \sum_i n_{\uparrow,\mathbf{r}_i} n_{\downarrow,\mathbf{r}_i}. \quad (1)$$

Here, $b^{\dagger}_{\sigma,\boldsymbol{r}_i}(b_{\sigma,\boldsymbol{r}_i})$ are creation (annihilation) operators at site i, and $n_{\sigma,\boldsymbol{r}_i} = b^{\dagger}_{\sigma,\boldsymbol{r}_i} b_{\sigma,\boldsymbol{r}_i}$ is the density operator. $t_1(t_2)$ is the amplitude of hopping to the first (second) neighbors, and $\nu^{\uparrow}_{ik} = -\nu^{\downarrow}_{ik} = 1(-1)$ for a left turn (right turn) on the honeycomb lattice. We assume a filling of one boson per site $\langle n_{\uparrow,\boldsymbol{r}_i} + n_{\downarrow,\boldsymbol{r}_i}\rangle = 1$. The Haldane model [40] for spinless fermions has been realized through Floquet engineering in cold atoms [59]. Similarly, spin-orbit models have been proposed in optical lattices setups [60–62] and experimentally achieved with photons [63–66]. All the ingredients required for a successful implementation of Eq. (1) are thus available.

I. B-DMFT on BKMH model.—The ground-state phase diagram of the BKMH model obtained from B-DMFT [48–53] is shown in Fig. 1(b). In order to address unusual states breaking translational symmetry, we use real-space B-DMFT [54,67–69]. Local effective problems represented by the Anderson impurity model are solved using exact diagonalization [54]. As found for the bosonic Haldane model at the same filling [70], three phases are competing: a uniform superfluid (SF), a chiral superfluid (CSF) and a Mott insulator (MI) (they are distinguished by the behaviors of the order parameter $\langle b_{\sigma,\boldsymbol{r}_i}\rangle$ and of the local currents $J^{\sigma}_{ij} = \mathfrak{Im}\langle b^{\dagger}_{\sigma,\boldsymbol{r}_i} b_{\sigma,\boldsymbol{r}_j}\rangle$ [54]).

We here focus on the MI phase. As shown in Fig. 1(b), the system enters the Mott phase when intraspecies (U) and interspecies ($U_{\uparrow\downarrow}$) interactions become strong enough. The internal structure of the MI phase is richer than in the bosonic Haldane model [70] and comprises different

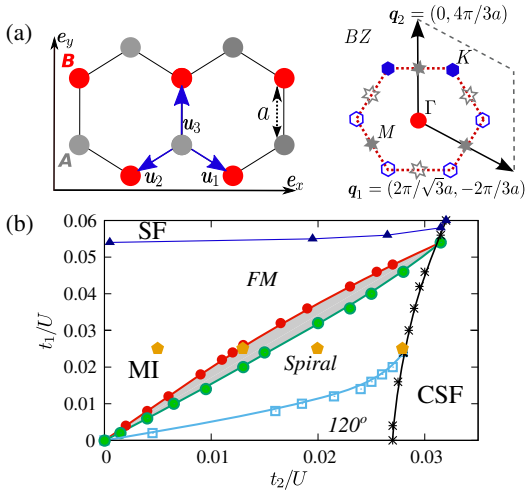

FIG. 1. (a) Honeycomb lattice and its first Brillouin zone. (b) Phase diagram of the BKMH model obtained using B-DMFT containing Mott insulator, uniform superfluid, and chiral superfluid phases with different regimes of the MI phase marked in italic. The central gray region corresponds to the states with no coplanar order. Parameters $U_{\uparrow\downarrow}/U = 0.5$, $\mu/U_{\uparrow\downarrow} = 0.5$, lattice of 96 sites. "Pentagons" mark parameter values that we further explore in Figs. 2(a)–2(d).

regimes. Applying standard perturbation theory [71], one rewrites the Hamiltonian (1) in terms of pseudospin-1/2 operators $S^{+}_{\boldsymbol{r}_i} = S^{x}_{\boldsymbol{r}_i} + iS^{y}_{\boldsymbol{r}_i} = b^{\dagger}_{\uparrow,\boldsymbol{r}_i} b_{\downarrow,\boldsymbol{r}_i}$, $S^{-}_{\boldsymbol{r}_i} = S^{x}_{\boldsymbol{r}_i} - iS^{y}_{\boldsymbol{r}_i} = b^{\dagger}_{\downarrow,\boldsymbol{r}_i} b_{\uparrow,\boldsymbol{r}_i}$ and $S^{z}_{\boldsymbol{r}_i} = (n_{\uparrow,\boldsymbol{r}_i} - n_{\downarrow,\boldsymbol{r}_i})/2$ as follows:

$$H = -\sum_{\langle ij\rangle}[J_1(S^{+}_{\boldsymbol{r}_i} S^{-}_{\boldsymbol{r}_j} + \text{H.c.}) - K_1 S^{z}_{\boldsymbol{r}_i} S^{z}_{\boldsymbol{r}_j}] + \sum_{\langle\langle ik\rangle\rangle}[J_2(S^{+}_{\boldsymbol{r}_i} S^{-}_{\boldsymbol{r}_k} + \text{H.c.}) + K_2 S^{z}_{\boldsymbol{r}_i} S^{z}_{\boldsymbol{r}_k}], \quad (2)$$

where $J_i = t_i^2/U_{\uparrow\downarrow}$ and $K_i = t_i^2(1/U_{\uparrow\downarrow} - 2/U)$. We observe that the spin-1/2 frustrated XY model is realized when $U = 2U_{\uparrow\downarrow}$ (for which $K_i = 0$). Frustration is associated with the positive sign of the J_2 term, which combines the sign of the bosonic exchange and the phase of π accumulated in the hoppings between second neighbors. The fermionic Kane-Mele model does not include such frustrating terms [56,72].

The properties of this effective XY model depend only on the ratio $J_2/J_1 = (t_2/t_1)^2$. In the classical limit, a coplanar ansatz [16,54,73] provides the following phase diagram: the ferromagnetic (FM) phase is stable for $J_2/J_1 \leq 1/6$, above which degenerate incommensurate spiral waves become energetically favored. Their wave vectors live on closed contours in the Brillouin zone. In the case of the Heisenberg model, quantum fluctuations were predicted to lift this degeneracy via an order-by-disorder mechanism [18].

B-DMFT on the BKMH model captures already deviations from this classical picture. In Figs. 2(a)–2(d), we study the coplanar spin ordering (arrows), in the presence of an external staggered magnetic field h_z, breaking the $\mathcal{P}$ symmetry (bond-center reflection which interchanges sublattices A and B):

$$H_z = h_z\left(\sum_{i\in A} S^{z}_{\boldsymbol{r}_i} - \sum_{j\in B} S^{z}_{\boldsymbol{r}_j}\right). \quad (3)$$

It corresponds to a staggered chemical potential in the boson language [74] and we will understand its role hereafter. We directly infer some of the ordered phases: at low J_2/J_1, all spins are aligned in a FM order, while at large J_2/J_1, we recover a 120° order. For $U_{\uparrow\downarrow}/U = 0.5, t_1/U = 0.025$ in the range $0.36 \lesssim J_2/J_1 \lesssim 1.23$ we observe a different configuration of spiral waves [Fig. 2(c)]. In addition, we find an exotic intermediate regime when $0.25 \lesssim J_2/J_1 \lesssim 0.36$ (we notice that positions of phase boundaries are affected by h_z), characterized by a chiral spin state (CSS) with no coplanar magnetic order [Fig. 2(b)]. This is reminiscent of the debated intermediate phase found in numerical studies on the XY model [31–38]. On the one hand, density matrix renormalization group [33,34] and coupled cluster method [35] results evidenced an antiferromagnetic Ising ordering, breaking $\mathcal{P}$ while preserving translational invariance. On the other hand, this observation was not reported in ED [31,32] nor variational Monte Carlo

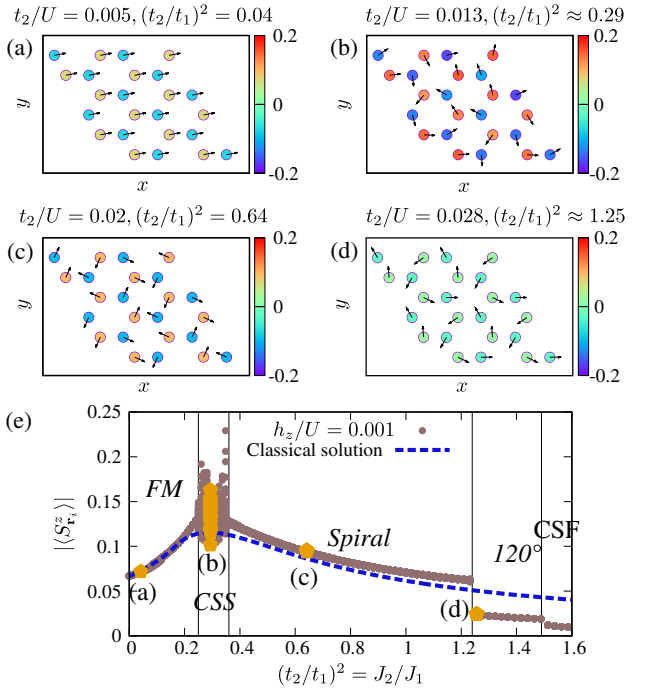

FIG. 2. Results of the B-DMFT for different values of $(t_2/t_1)^2 = J_2/J_1$ for $h_z/U = 10^{-3}$, $U_{\uparrow\downarrow}/U = 0.5$, $t_1/U = 0.025$ on a lattice of 24 sites. (a)–(d) Different spin configurations. The color palette gives $\langle S^z_{r_i}\rangle$, while arrows depict ordering in the xy plane. (a) Uniform state with ferromagnetic ordering; (b) chiral spin state with no coplanar order; (c) a configuration of spiral states, in which each pseudospin is aligned with only one of its three first neighbors and antialigned with two of its six second neighbors; (d) a 120° configuration. (e) Absolute value of $|\langle S^z_{r_i}\rangle|$. For each ratio $(t_2/t_1)^2$ we plot the result for all 24 sites and compare it to the classical solution. Pentagons mark results presented in (a)–(d). Note that for finite values of h_z the border between the 120° Mott state and CSF is slightly shifted in favor of the Mott state.

[36–38] analyses, raising questions about the exact nature of this intermediate phase.

Mapping the model onto a fermionic one and performing a mean-field analysis [39,54], it was proposed that an intermediate frustration stabilizes a phase with spontaneously broken $\mathcal{P}$ and $\mathcal{T}$. This phase is characterized by antiferromagnetic correlations and ChS fluxes staggered within the unit cell as in the celebrated Haldane model [40] and the authors suggested that it realizes the chiral spin liquid state of Kalmeyer-Laughlin [75,76]. In this context, we plot in Fig. 2(e), the response for the magnetization $\langle S^z_{r_i}\rangle$ with respect to the field h_z. All phases except the CSS are characterized by a trivial response to the perturbation: $\langle S^z_{r_i}\rangle \sim h_z$, whereas $\langle S^z_{r_i}\rangle$ is strongly fluctuating in the CSS (however we do not observe spontaneous symmetry breaking with B-DMFT). These results cannot be explained in the context of a simple coplanar ansatz, but could be related to a breaking of the degeneracy between two mean-field solutions in the ChS field theory description [54].

II. ED on frustrated XY model.—We complete the study of the effective frustrated XY model using ED and previously unaddressed probes such as the responses to $\mathcal{P}$ and $\mathcal{T}$ breaking perturbations and the topological description of the ground state. We consider lattices of 24–32 sites, with periodic boundary conditions, and fixed total magnetization $S^z_{\rm tot} = 0$ if not stated otherwise. First, phase boundaries are derived from the maxima of fidelity metric g [54], which probes the first derivative of the ground-state wave function [77–79]. The phase diagram of the XY model deduced from the ED calculations is given in Fig. 3(a). In agreement with the B-DMFT and previous numerical studies, we observe three phase transitions at $J_2/J_1 \approx 0.21, 0.36$, and 1.32. Small deviations in these values from the B-DMFT results could be due to the finite size of ED clusters or nonperturbative interaction effects (the XY model does not describe correctly the physics of the Mott phase when t_i/U are too large). The nature of the phases detected with ED is verified by looking at the coplanar static structure factor

$$S_{\rm Spiral}(\boldsymbol{q}) = 2\sum_{i,j\in A} e^{i\boldsymbol{q}\cdot(\boldsymbol{r}_i-\boldsymbol{r}_j)}\langle S^x_{\boldsymbol{r}_i} S^x_{\boldsymbol{r}_j}\rangle. \tag{4}$$

Spiral waves display a maximum of $S_{\rm Spiral}$ at some wave vector(s) $\boldsymbol{q}$ in the first Brillouin zone. We observe [54] that the phase in the region $J_2/J_1 \lesssim 0.21$ corresponds to FM order since $S_{\rm spiral}$ has a peak at $\boldsymbol{q} = \boldsymbol{\Gamma}$. The phase at

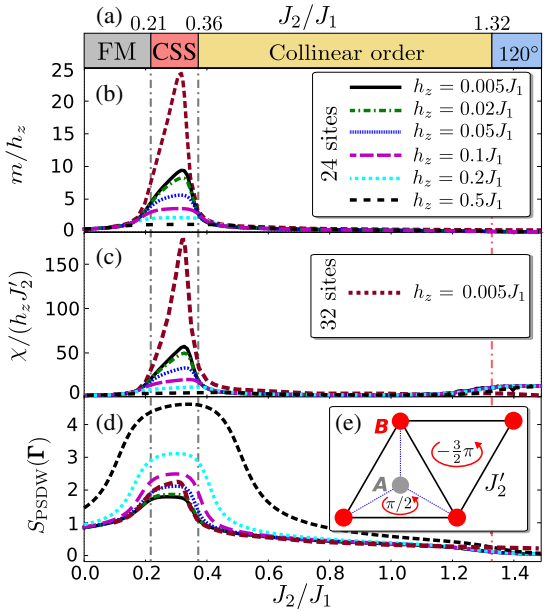

FIG. 3. Results of the ED. (a) Phase diagram of the frustrated XY model. (b)–(d) Variation of the observables with the dimensionless parameter J_2/J_1 for different values of h_z, with $J_2' = 0.01J_1$, on a lattice of 6×2 unit cells. (b) Difference of the average Ising magnetization on two sublattices m. (c) Scalar spin chirality χ. (d) Pseudospin density wave structure factor $S_{\rm PSDW}(\boldsymbol{\Gamma})$. (e) Schematic representation of the perturbation term $H_{J_2'}$.

$0.36 \lesssim J_2/J_1 \lesssim 1.32$ corresponds to a spiral wave with collinear order (structure factor has maxima at three $\boldsymbol{M}$ points) as expected from the order by disorder mechanism. At $1.32 \lesssim J_2/J_1$ the ground state is the 120° order spiral wave (structure factor has a peak at two Dirac points $\boldsymbol{K}$). In the intermediate frustration regime ($0.21 \lesssim J_2/J_1 \lesssim 0.36$) S_{spiral} is flat in reciprocal space and we expect the ground state to be disordered in the xy plane. We notice that the exact positions of the phase transitions, especially collinear order $\leftrightarrow$ 120° order, are sensitive to the lattice choice [54]. The ground state in all phases is located in the same sector of the total momentum at point $\boldsymbol{\Gamma}$. Based on the ChS field theory predictions, the order-by-disorder arguments and numerical observations, the CSS $\leftrightarrow$ collinear order, and collinear order $\leftrightarrow$ 120° order phase transitions are expected to be first order, whereas the FM $\leftrightarrow$ CSS phase transition to be second order.

We analyze the linear response to perturbations breaking $\mathcal{P}$ and $\mathcal{T}$. We are interested in the relative magnetization between the two sublattices $m = \langle m_{\boldsymbol{r}_i} \rangle = \langle S^z_{\boldsymbol{r}_i} - S^z_{\boldsymbol{r}_i+\boldsymbol{u}_3} \rangle$, as well as the scalar spin chirality $\chi = \langle \boldsymbol{S}_{\boldsymbol{r}_i} \cdot (\boldsymbol{S}_{\boldsymbol{r}_i+\boldsymbol{u}_1} \times \boldsymbol{S}_{\boldsymbol{r}_i+\boldsymbol{u}_2}) \rangle$. Here we suppose that $i \in A$ and $\boldsymbol{u}_i$ are vectors between first neighbor sites defined in Fig. 1(a). When calculating the chirality χ, we add a perturbation corresponding to the second-neighbor hopping of the Haldane model, of amplitude J_2' and phase $\pi/2$ [as shown in Fig. 3(e)]:

$$H_{J_2'} = J_2' \sum_{\langle\langle ik \rangle\rangle} (e^{\pm i\pi/2} S^+_{\boldsymbol{r}_i} S^-_{\boldsymbol{r}_k} + \text{H.c.}). \tag{5}$$

We are interested in the limit $h_z, J_2' \ll J_1$. Results of the ED calculations are presented in Figs. 3(b)–3(c). The CSS reveals itself by sharp responses to such external fields. Moreover, the scaled quantities m/h_z and $\chi/(h_z J_2')$ tend to diverge when h_z, $J_2' \to 0$, giving a strong indication for spontaneous symmetry breaking. This justifies our definition of the CSS, the properties of which can be observed experimentally by tracking on-site populations of bosons $n_{\sigma \boldsymbol{r}_i}$ and currents $J^{\sigma}_{ij} = \mathfrak{Im} \langle b^{\dagger}_{\sigma \boldsymbol{r}_i} b_{\sigma \boldsymbol{r}_j} \rangle$ [80]. One can probe the antiferromagnetic ordering without breaking $\mathcal{P}$ and $\mathcal{T}$ by calculating the pseudospin density wave (PSDW) structure factor [31,32]:

$$S_{\text{PSDW}}(\boldsymbol{q}) = \sum_{i,j} e^{i\boldsymbol{q}\cdot(\boldsymbol{r}_i - \boldsymbol{r}_j)} \langle m_{\boldsymbol{r}_i} m_{\boldsymbol{r}_j} \rangle. \tag{6}$$

We observe in Fig. 3(d) that $S_{\text{PSDW}}(\boldsymbol{q})$ has a peak at $\boldsymbol{q} = \boldsymbol{\Gamma}$ in the intermediate frustration regime. These features are hardly affected by moderate Ising interactions $K_i/J_1 \sim 0.1$ in Eq. (2) [81].

The observed spin configuration of the CSS could describe the chiral spin liquid of Kalmeyer and Laughlin [75,76]. Yet, we know that chiral spin liquids are characterized by a topological degeneracy in the thermodynamic limit on a compact space [82–84]. In a two-dimensional system with periodic boundaries one should have a fourfold degenerate ground state with two topological degeneracies per chirality sector. Still, because of finite size effects, one only expects an approximate degeneracy in simulations.

In Figs. 4(a)–4(b), we show the low-energy spectrum as a function of J_2/J_1, resolved in different sectors of total momentum $\boldsymbol{Q}$. As mentioned previously, the ground state always belongs to the sector $\boldsymbol{Q} = \boldsymbol{\Gamma}$. In the intermediate frustration regime, we observe the onset of a gapped doubly degenerate ground-state manifold. The first excited state has the same momentum $\boldsymbol{Q} = \boldsymbol{\Gamma}$, but lies in the opposite sector of $\mathcal{P}$. The first excited state also moves away in energy when the perturbations H_z and $H_{J_2'}$ are switched on.

We probe the robustness of the low energy quasidegenerate state sector by performing Laughlin's gedanken experiment and pumping a quantum of magnetic flux through one of the nontrivial loops of the torus [85–87]. Numerically, this is achieved using twisted boundary conditions in a translational symmetry preserving manner. The results are given in Fig. 4(c). We observe that the same states in the sector $\boldsymbol{Q} = \boldsymbol{\Gamma}$ are nontrivially gapped for all twists. For the pumping of a single flux quantum we could not observe a spectral flow in the ground-state manifold, that, however, does not imply that the manifold is topologically trivial [88–90]. The topological nature of the ground-state manifold is unambiguously determined by calculating the Chern number [91–94]:

$$C = \frac{1}{2\pi} \int_0^{2\pi} \int_0^{2\pi} B(\theta_1, \theta_2) d\theta_1 d\theta_2. \tag{7}$$

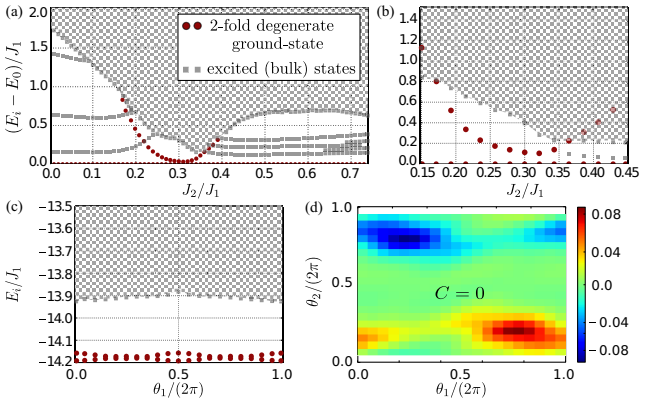

FIG. 4. ED calculations of the low energy spectra as a function of J_2/J_1 showing (using red circles) the formation of a quasidegenerate twofold ground-state manifold (a) on a lattice of 4×3 unit cells for various S^z_{Tot}; (b) on a lattice of 4×4 unit cells in the $S^z_{\text{Tot}} = 0$ sector only. (c) Low energy spectrum as a function of the twist angle θ_1 for $J_2/J_1 = 0.3$ and $\theta_2 = 0$ on a lattice of 4×3 unit cells. (d) Berry curvature calculated using the non-Abelian formalism resulting in a vanishing Chern number shown for $J_2/J_1 = 0.3$, $h_z/J_1 = J_2'/J_1 = 0.02$ on a lattice of 4×3 unit cells.

Here θ_1 and θ_2 are two angles of twisted boundary conditions and $B(\theta_1,\theta_2)$ is the Berry curvature [95]. We notice that two phases θ_i ($i=1,2$) introduced in the spin language would correspond to four phases θ_i^σ in the language of bosons of the BKMH model, for which the spin component $\theta_i^\uparrow-\theta_i^\downarrow=\theta_i$ is fixed and the $U(1)$ component $\theta_i^\uparrow+\theta_i^\downarrow$ is free [96]. Since the two quasidegenerate ground states lie in the same symmetry sector and cannot be separated unless twists are trivial ($\mathcal{P}$ cannot be used with twisted boundary conditions), we evaluate the Berry curvature using the gauge-invariant non-Abelian formulation [97–99]: $B(\theta_1,\theta_2)\delta\theta_1\delta\theta_2=\mathfrak{Im}\ln\mathfrak{Det}[\mathcal{M}(\theta_1,\theta_2)]$, where elements of the matrix $\mathcal{M}$ are obtained as follows:

$$\begin{aligned}\mathcal{M}_{ij}(\theta_1,\theta_2)=&\langle\phi_i(\theta_1,\theta_2)|\phi_{\mu_1}(\theta_1+\delta\theta_1,\theta_2)\rangle\\&\times\langle\phi_{\mu_1}(\theta_1+\delta\theta_1,\theta_2)|\phi_{\mu_2}(\theta_1+\delta\theta_1,\theta_2+\delta\theta_2)\rangle\\&\times\langle\phi_{\mu_2}(\theta_1+\delta\theta_1,\theta_2+\delta\theta_2)|\phi_{\mu_3}(\theta_1,\theta_2+\delta\theta_2)\rangle\\&\times\langle\phi_{\mu_3}(\theta_1,\theta_2+\delta\theta_2)|\phi_j(\theta_1,\theta_2)\rangle.\end{aligned}\tag{8}$$

Here, $\delta\theta_1$ and $\delta\theta_2$ refer to the numerical mesh along the θ_1 and θ_2. $i,j,\mu_i=1,2$ are indices of states $|\phi_1\rangle$ and $|\phi_2\rangle$ in the ground-state manifold and the summation over μ_i is implicit. In Fig. 4(d), we show a typical shape of the Berry curvature. We find that the Chern number is zero in the intermediate frustration regime. This result suggests that the intermediate phase in the frustrated XY model is most likely to be a CSS with no topological order, as suggested in Refs. [33–35], and not the Kalmeyer-Laughlin state, with gauge fluctuations beyond the mean-field solution making the phase topologically trivial as in the fermionic Kane-Mele model [56–58].

To conclude, we studied the phase diagram of the bosonic Kane-Mele-Hubbard model on the honeycomb lattice. We have shown that an effective frustrated XY model appears in the Mott insulator phase. This model possesses an intermediate frustration regime with a nontrivial chiral spin state, which breaks both $\mathcal{P}$ and $\mathcal{T}$. It displays a finite scalar spin chirality order and an antiferromagnetic Ising ordering, while remaining translationally invariant. Measuring the Chern number associated with this state reveals its nontopological nature.

We thank Loïc Herviou, Grégoire Misguich, Stephan Rachel, Cécile Repellin, and Tigran Sedrakyan for insightful discussions. This work has benefitted from discussions at CIFAR meetings in Canada and Société Française de Physique. Support by the Deutsche Forschungsgemeinschaft via DFG FOR 2414, DFG SPP 1929 GiRyd, and the high-performance computing center LOEWE-CSC is gratefully acknowledged. This work was supported in part by DAAD (German Academic and Exchange Service) under project BKMH. I. V. acknowledges support by the Ministry of Education, Science, and Technological Development of the Republic of Serbia under projects ON171017 and BKMH, and by the European Commission under H2020 project VI-SEEM, Grant No. 675121. Numerical simulations were partly run on the PARADOX supercomputing facility at the Scientific Computing Laboratory of the Institute of Physics Belgrade. K. L. H. acknowledges support from PALM Labex, Paris-Saclay, Grant No. ANR-10-LABX-0039.

[1] C. Lhuillier and G. Misguich, in *High Magnetic Fields: Applications in Condensed Matter Physics and Spectroscopy*, edited by C. Berthier, L. P. Lévy, and G. Martinez (Springer, Berlin, Heidelberg, 2002), p. 161.
[2] L. Balents, Nature (London) **464**, 199 (2010).
[3] M. R. Norman, Rev. Mod. Phys. **88**, 041002 (2016).
[4] L. Savary and L. Balents, Rep. Prog. Phys. **80**, 016502 (2017).
[5] P. Lecheminant, B. Bernu, C. Lhuillier, L. Pierre, and P. Sindzingre, Phys. Rev. B **56**, 2521 (1997).
[6] S. Yan, D. A. Huse, and S. R. White, Science **332**, 1173 (2011).
[7] S. Depenbrock, I. P. McCulloch, and U. Schollwöck, Phys. Rev. Lett. **109**, 067201 (2012).
[8] B. Fåk, E. Kermarrec, L. Messio, B. Bernu, C. Lhuillier, F. Bert, P. Mendels, B. Koteswararao, F. Bouquet, J. Ollivier, A. D. Hillier, A. Amato, R. H. Colman, and A. S. Wills, Phys. Rev. Lett. **109**, 037208 (2012).
[9] H. J. Schulz and T. A. L. Ziman, Europhys. Lett. **18**, 355 (1992).
[10] H. J. Schulz, T. A. L. Ziman, and D. Poilblanc, J. Phys. I (France) **6**, 675 (1996).
[11] A. Kitaev, Ann. Phys. (Amsterdam) **321**, 2 (2006).
[12] Z. Y. Meng, T. C. Lang, S. Wessel, F. F. Assaad, and A. Muramatsu, Nature (London) **464**, 847 (2010).
[13] S. Sorella, Y. Otsuka, and S. Yunoki, Sci. Rep. **2**, 992 (2012).
[14] F. F. Assaad and I. F. Herbut, Phys. Rev. X **3**, 031010 (2013).
[15] R. Flint and P. A. Lee, Phys. Rev. Lett. **111**, 217201 (2013).
[16] J. Fouet, P. Sindzingre, and C. Lhuillier, Eur. Phys. J. B **20**, 241 (2001).
[17] F. Wang, Phys. Rev. B **82**, 024419 (2010).
[18] A. Mulder, R. Ganesh, L. Capriotti, and A. Paramekanti, Phys. Rev. B **81**, 214419 (2010).
[19] B. K. Clark, D. A. Abanin, and S. L. Sondhi, Phys. Rev. Lett. **107**, 087204 (2011).
[20] A. F. Albuquerque, D. Schwandt, B. Hetényi, S. Capponi, M. Mambrini, and A. M. Läuchli, Phys. Rev. B **84**, 024406 (2011).
[21] D. C. Cabra, C. A. Lamas, and H. D. Rosales, Phys. Rev. B **83**, 094506 (2011).
[22] J. Reuther, D. A. Abanin, and R. Thomale, Phys. Rev. B **84**, 014417 (2011).
[23] F. Mezzacapo and M. Boninsegni, Phys. Rev. B **85**, 060402 (2012).
[24] H. Zhang and C. A. Lamas, Phys. Rev. B **87**, 024415 (2013).
[25] R. Ganesh, J. van den Brink, and S. Nishimoto, Phys. Rev. Lett. **110**, 127203 (2013).
[26] S.-S. Gong, D. N. Sheng, O. I. Motrunich, and M. P. A. Fisher, Phys. Rev. B **88**, 165138 (2013).

[27] Z. Zhu, D. A. Huse, and S. R. White, Phys. Rev. Lett. **110**, 127205 (2013).
[28] S.-S. Gong, W. Zhu, L. Balents, and D. N. Sheng, Phys. Rev. B **91**, 075112 (2015).
[29] F. Ferrari, S. Bieri, and F. Becca, Phys. Rev. B **96**, 104401 (2017).
[30] H. S. Nair, J. M. Brown, E. Coldren, G. Hester, M. P. Gelfand, A. Podlesnyak, Q. Huang, and K. A. Ross, arXiv:1712.06208.
[31] C. N. Varney, K. Sun, V. Galitski, and M. Rigol, Phys. Rev. Lett. **107**, 077201 (2011).
[32] C. N. Varney, K. Sun, V. Galitski, and M. Rigol, New J. Phys. **14**, 115028 (2012).
[33] Z. Zhu, D. A. Huse, and S. R. White, Phys. Rev. Lett. **111**, 257201 (2013).
[34] Z. Zhu and S. R. White, Mod. Phys. Lett. B **28**, 1430016 (2014).
[35] R. F. Bishop, P. H. Y. Li, and C. E. Campbell, Phys. Rev. B **89**, 214413 (2014).
[36] J. Carrasquilla, A. DiCiolo, F. Becca, V. Galitski, and M. Rigol, Phys. Rev. B **88**, 241109 (2013).
[37] A. Di Ciolo, J. Carrasquilla, F. Becca, M. Rigol, and V. Galitski, Phys. Rev. B **89**, 094413 (2014).
[38] T. Nakafuji and I. Ichinose, Phys. Rev. A **96**, 013628 (2017).
[39] T. A. Sedrakyan, L. I. Glazman, and A. Kamenev, Phys. Rev. Lett. **114**, 037203 (2015).
[40] F. D. M. Haldane, Phys. Rev. Lett. **61**, 2015 (1988).
[41] E. Fradkin, Phys. Rev. Lett. **63**, 322 (1989).
[42] J. Ambjørn and G. Semenoff, Phys. Lett. B **226**, 107 (1989).
[43] A. Lopez, A. G. Rojo, and E. Fradkin, Phys. Rev. B **49**, 15139 (1994).
[44] G. Misguich, T. Jolicoeur, and S. M. Girvin, Phys. Rev. Lett. **87**, 097203 (2001).
[45] K. Sun, K. Kumar, and E. Fradkin, Phys. Rev. B **92**, 115148 (2015).
[46] I. Bloch, J. Dalibard, and S. Nascimbene, Nat. Phys. **8**, 267 (2012).
[47] N. Goldman, J. C. Budich, and P. Zoller, Nat. Phys. **12**, 639 (2016).
[48] A. Georges, G. Kotliar, W. Krauth, and M. J. Rozenberg, Rev. Mod. Phys. **68**, 13 (1996).
[49] K. Byczuk and D. Vollhardt, Phys. Rev. B **77**, 235106 (2008).
[50] W.-J. Hu and N.-H. Tong, Phys. Rev. B **80**, 245110 (2009).
[51] A. Hubener, M. Snoek, and W. Hofstetter, Phys. Rev. B **80**, 245109 (2009).
[52] P. Anders, E. Gull, L. Pollet, M. Troyer, and P. Werner, Phys. Rev. Lett. **105**, 096402 (2010).
[53] M. Snoek and W. Hofstetter, in Quantum Gases: Finite Temperature and Non-Equilibrium Dynamics, edited by N. Proukakis *et al.* (World Scientific, Singapore, 2013), p. 355.
[54] See Supplemental Material at http://link.aps.org/supplemental/10.1103/PhysRevLett.120.157201 for (i) details on the B-DMFT method; plots of the order parameters across the superfluid (SF and CSF)—Mott insulator phase transitions; (ii) classical solution of the spin model with and without applied external magnetic field; (iii) mean-field treatment of the spin model using Chern-Simons field theory; (iv) details on the ED measurement of the fidelity and the static structure factors; comparison of the lattices of 6×2, 4×3 and 4×4 unit cells.
[55] C. L. Kane and E. J. Mele, Phys. Rev. Lett. **95**, 226801 (2005).
[56] S. Rachel and K. Le Hur, Phys. Rev. B **82**, 075106 (2010).
[57] W. Wu, S. Rachel, W.-M. Liu, and K. Le Hur, Phys. Rev. B **85**, 205102 (2012).
[58] M. Hohenadler, Z. Y. Meng, T. C. Lang, S. Wessel, A. Muramatsu, and F. F. Assaad, Phys. Rev. B **85**, 115132 (2012).
[59] G. Jotzu, M. Messer, R. Desbuquois, M. Lebrat, T. Uehlinger, D. Greif, and T. Esslinger, Nature (London) **515**, 237 (2014).
[60] C. J. Kennedy, G. A. Siviloglou, H. Miyake, W. C. Burton, and W. Ketterle, Phys. Rev. Lett. **111**, 225301 (2013).
[61] J. Struck, J. Simonet, and K. Sengstock, Phys. Rev. A **90**, 031601 (2014).
[62] Z. Yan, B. Li, X. Yang, and S. Wan, Sci. Rep. **5**, 16197 (2015).
[63] M. Hafezi, E. A. Demler, M. D. Lukin, and J. M. Taylor, Nat. Phys. **7**, 907 (2011).
[64] V. G. Sala, D. D. Solnyshkov, I. Carusotto, T. Jacqmin, A. Lemaître, H. Terças, A. Nalitov, M. Abbarchi, E. Galopin, I. Sagnes, J. Bloch, G. Malpuech, and A. Amo, Phys. Rev. X **5**, 011034 (2015).
[65] L. Lu, J. D. Joannopoulos, and M. Soljacic, Nat. Photonics **8**, 821 (2014).
[66] K. Le Hur, L. Henriet, A. Petrescu, K. Plekhanov, G. Roux, and M. Schiró, C.R. Phys. **17**, 808 (2016).
[67] Y. Li, M. R. Bakhtiari, L. He, and W. Hofstetter, Phys. Rev. B **84**, 144411 (2011).
[68] L. He, Y. Li, E. Altman, and W. Hofstetter, Phys. Rev. A **86**, 043620 (2012).
[69] L. He, A. Ji, and W. Hofstetter, Phys. Rev. A **92**, 023630 (2015).
[70] I. Vasić, A. Petrescu, K. Le Hur, and W. Hofstetter, Phys. Rev. B **91**, 094502 (2015).
[71] A. B. Kuklov and B. V. Svistunov, Phys. Rev. Lett. **90**, 100401 (2003).
[72] M. W. Young, S.-S. Lee, and C. Kallin, Phys. Rev. B **78**, 125316 (2008).
[73] E. Rastelli, A. Tassi, and L. Reatto, Physica (Amsterdam) **97B+C**, 1 (1979).
[74] G. W. Semenoff, Phys. Rev. Lett. **53**, 2449 (1984).
[75] V. Kalmeyer and R. B. Laughlin, Phys. Rev. Lett. **59**, 2095 (1987).
[76] V. Kalmeyer and R. B. Laughlin, Phys. Rev. B **39**, 11879 (1989).
[77] P. Zanardi and N. Paunković, Phys. Rev. E **74**, 031123 (2006).
[78] S.-J. Gu, Int. J. Mod. Phys. B **24**, 4371 (2010).
[79] C. N. Varney, K. Sun, M. Rigol, and V. Galitski, Phys. Rev. B **82**, 115125 (2010).
[80] M. Atala, M. Aidelsburger, M. Lohse, J. T. Barreiro, B. Paredes, and I. Bloch, Nat. Phys. **10**, 588 (2014).
[81] P. H. Y. Li, R. F. Bishop, and C. E. Campbell, Phys. Rev. B **89**, 220408 (2014).
[82] X. G. Wen, F. Wilczek, and A. Zee, Phys. Rev. B **39**, 11413 (1989).
[83] X. G. Wen, Phys. Rev. B **40**, 7387 (1989).

[84] X.-G. Wen, Adv. Phys. **44**, 405 (1995).
[85] R. B. Laughlin, Phys. Rev. B **23**, 5632 (1981).
[86] R. B. Laughlin, Phys. Rev. Lett. **50**, 1395 (1983).
[87] D. J. Thouless, Phys. Rev. B **40**, 12034 (1989).
[88] Y.-F. Wang, Z.-C. Gu, C.-D. Gong, and D. N. Sheng, Phys. Rev. Lett. **107**, 146803 (2011).
[89] C. Hickey, L. Cincio, and Z. Papić, and A. Paramekanti, Phys. Rev. Lett. **116**, 137202 (2016).
[90] K. Kumar, H. J. Changlani, B. K. Clark, and E. Fradkin, Phys. Rev. B **94**, 134410 (2016).
[91] Q. Niu, D. J. Thouless, and Y.-S. Wu, Phys. Rev. B **31**, 3372 (1985).
[92] M. Kohmoto, Ann. Phys. (N.Y.) **160**, 343 (1985).
[93] Y. Hatsugai, J. Phys. Soc. Jpn. **73**, 2604 (2004).
[94] Y. Hatsugai, J. Phys. Soc. Jpn. **74**, 1374 (2005).
[95] M. V. Berry, Proc. R. Soc. A **392**, 45 (1984).
[96] L. Fu and C. L. Kane, Phys. Rev. B **74**, 195312 (2006).
[97] R. Yu, X. L. Qi, A. Bernevig, Z. Fang, and X. Dai, Phys. Rev. B **84**, 075119 (2011).
[98] H. Shapourian and B. K. Clark, Phys. Rev. B **93**, 035125 (2016).
[99] K. Kumar, H. J. Changlani, B. K. Clark, and E. Fradkin, Phys. Rev. B **94**, 134410 (2016).